Energies **2012**, *5*, 4268-4287; doi:10.3390/en5114268

OPEN ACCESS

energies

ISSN 1996-1073

www.mdpi.com/journal/energies

Article

Exergy Analysis of an Intermediate Temperature Solid Oxide Fuel Cell-Gas Turbine Hybrid System Fed with Ethanol

Anastassios Stamatis, Christina Vinni, Diamantis Bakalis, Fotini Tzorbatzoglou and Panagiotis Tsiakaras *

Department of Mechanical Engineering, School of Engineering, University of Thessaly, Pedion Areos, 38334, Greece; E-Mails: tastamat@uth.gr (A.S.); vinni@uth.gr (C.V.); dbakalis@uth.gr (D.B.); fotinitzo@uth.gr (F.T.)

* Author to whom correspondence should be addressed; E-Mail: tsiak@uth.gr; Tel.: +30-24210-74065/74081; Fax: +30-24210-74050.

Received: 10 July 2012; in revised form: 24 September 2012 / Accepted: 18 October 2012 / Published: 24 October 2012

Abstract: In the present work, an ethanol fed Solid Oxide Fuel Cell-Gas Turbine (SOFC-GT) system has been parametrically analyzed in terms of exergy and compared with a single SOFC system. The solid oxide fuel cell was fed with hydrogen produced from ethanol steam reforming. The hydrogen utilization factor values were kept between 0.7 and 1. The SOFC's Current-Volt performance was considered in the range of 0.1–3 A/cm^2 at 0.9–0.3 V, respectively, and at the intermediate operating temperatures of 550 and 600 °C, respectively. The curves used represent experimental results obtained from the available bibliography. Results indicated that for low current density values the single SOFC system prevails over the SOFC-GT hybrid system in terms of exergy efficiency, while at higher current density values the latter is more efficient. It was found that as the value of the utilization factor increases the SOFC system becomes more efficient than the SOFC-GT system over a wider range of current density values. It was also revealed that at high current density values the increase of SOFC operation temperature leads in both cases to higher system efficiency values.

Keywords: exergy analysis; ethanol; SOFC-GT; fuel cell; hybrid systems

Nomenclature:

A_c	Fuel cell stack area (m^2)	s	Specific entropy (kJ/kg·K)
e	Specific exergy (kJ/kg)	T	Temperature (K)
$\dot{E}$	Exergy rate (kW)	U	Utilization factor
h	Specific enthalpy (kJ/kg)	V	Voltage (V)
i	Current density (A/m^2)	$\dot{W}$	Power (kW)
LHV	Lower heating value (kJ/kg)	x	Mole fraction
$\dot{m}$	Mass flow rate (kg/s)	ε	Effectiveness
$\dot{Q}$	Thermal energy (kW)	η	Isentropic efficiency
r_p	Pressure ratio	η_{II}	Exergy efficiency

Subscripts

1...12	Station numbering	*FC*	Fuel cell
a	Air	*g*	Exhaust gas
B	Burner	*i*	Inlet
C	Compressor	*o*	Reference
D	Destruction	*R*	Reformer
e	Exhaust	*Rec*	Recuperator
Et	Ethanol	*stoic*	Stoichiometric
Ev	Evaporator	*w*	Water
f	Fuel		

1. Introduction

The majority of current energy needs is supplied by combustion of non-renewable energy sources such as fossil fuels, which is associated with the release of large quantities of greenhouse gases, especially carbon dioxide (CO_2), and other harmful emissions to the atmosphere. Energy demand is increasing at an exponential rate, leading to a gradual depletion of the fossil fuels. This fact, combined with the efforts against pollution and greenhouse gas emissions, has led to considerable interest in using alternative sources of energy [1].

An answer to the above consideration could be hydrogen, which is considered to be the energy carrier of the future as it can play a major role in reducing harmful environmental emissions [2]. Nevertheless, nowadays most of hydrogen produced derives from fossil-based materials. Therefore, a renewable and clean energy source for hydrogen production seems to be necessary. Ethanol is a promising source of hydrogen as it is produced from biomass in a renewable way providing a closed carbon loop. Moreover ethanol has high hydrogen content and low toxicity [3].

The hydrogen produced from ethanol can be fed to alternative energy conversion systems such as fuel cells. It is well known that fuel cells are electrochemical devices that can directly convert chemical energy (*i.e.*, hydrogen) into electricity. Solid Oxide Fuel Cells (SOFCs) are currently the highest-temperature fuel cell in development and can be operated over a temperature range from 800 to

1100 °C so as to be highly efficient. During the last few years, many theoretical studies have appeared in the literature concerning Solid Oxide Fuel Cell systems [4–7] and Solid Oxide Fuel Cell combined with Gas Turbine (SOFC-GT) power cycles [8–15]. Most of these works have been devoted to high temperature SOFC systems fuelled by methane [12,13] and only very few of them concerned ethanol-fed SOFC-GT systems [14].

Srisiriwat [16] proposed a high temperature (1200 K) operation SOFC-GT combined system, integrated with an autothermal reformer and fed with ethanol for power generation. Also, Cocco *et al.* [17] demonstrated that alternative hydrogen carriers such as ethanol are very attractive fuels for SOFC-GT systems. Douvartzides *et al*. [18] tried to optimize ethanol-fed SOFC-based systems in terms of energy and exergy. Thermodynamic analysis for a solid oxide fuel cell with direct internal reforming fueled by ethanol has been performed in [19]. Performance of ethanol-fuelled solid oxide fuel cells was also investigated in terms of conductors used [20]. Casas *et al.* [21] recently studied a SOFC system integrated with an ethanol steam reforming unit using detailed model of all components of the plant, with a special attention to the kinetics of the ethanol steam reforming. Zhe *et al*. [22] also studied an ITSOFC co-generation system fueled by ethanol. Nevertheless, all the above works are based on theoretical models for the prediction of fuel cell performance. Low and intermediate temperature SOFCs have received considerable attention recently due to the improved stability, reliability and reduced cost. Moreover, SOFCs' operation at lower temperatures could: (a) enable the use of inexpensive metal components as inter-connects, (b) enhance the stability and durability of all the components and (c) offer the potential of more rapid start-up and shutdown procedure [23].

Taking into consideration that novel materials have recently been developed for intermediate temperature solid oxide fuel cells (with peak power density of ~1 W/cm^2 at 600 °C [24]), in the present investigation a mathematical model has been developed. The model simulates—from energy and exergy point of view—the operation of an intermediate temperature solid oxide fuel cell integrated with a conventional gas turbine (IT-SOFC-GT). It is the first time to our knowledge that experimental results for an intermediate temperature fuel cell performance taken from the open literature are used. Another aspect of this work is the exergetic comparison of a single ITSOFC system with an ITSOFC-GT system in order to investigate operating conditions where a hybrid system prevails in terms of efficiency.

2. Systems Description

In the present work two different configurations were analyzed and compared in terms of exergy efficiency: (a) a SOFC-GT system consisted of a SOFC stack, a compressor, a recuperator, a burner-reformer device, an evaporator and a turbine and (b) a single SOFC system consisting of a SOFC stack, a recuperator, a burner-reformer device and an evaporator. The considered configurations for both systems are presented in Figure 1.

Figure 1. Systems' configurations (**a**) SOFC-GT and (**b**) SOFC.

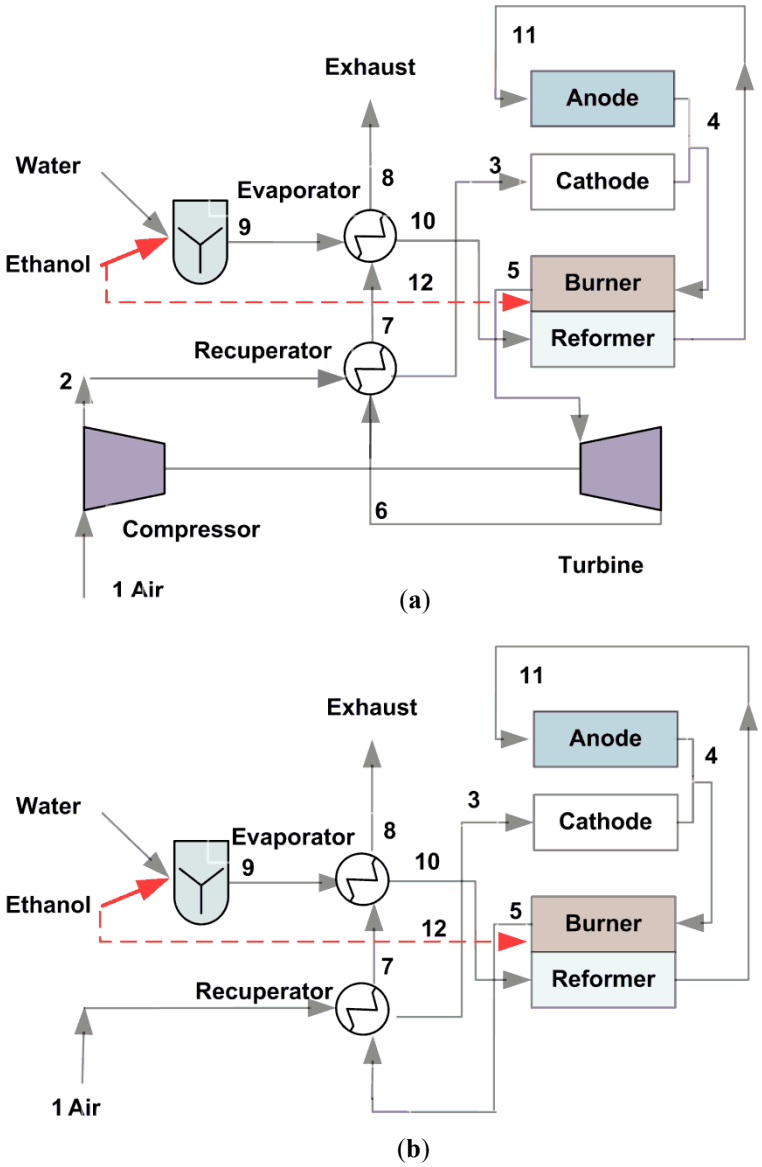

In the SOFC-GT system: air (1) is firstly compressed, (2) then is preheated at the recuperator at the operating temperature of the fuel cell (3) and enters the SOFC stack's cathode. A liquid ethanol and water mixture (9), after being evaporated (10), enters the reformer where ethanol is completely externally reformed and converted into hydrogen rich gas (11) and then enters the SOFC stack's anode. In the fuel cell the electrochemical reaction where heat and electricity are produced takes place. The fuel cell's products (4) enter the burner where the un-reacted hydrogen is burnt. As additional heat is required for the operation of the plant additional ethanol is separately fed into the burner and is directly combusted. The hot exhaust burner-reformer's products (5) are then expanded through the turbine. Finally, the exhaust gas (6) provides the heat required for (i) the inlet air preheated in the recuperator (7) and (ii) the liquid mixture evaporating in the evaporator, and then is discharged to the environment (8). The operation of the single SOFC system is similar. In this case the inlet air is preheated without being compressed, while the exhaust burner's product is directly fed to the recuperator.

3. System Modeling

The thermodynamic properties of each compound of the gas streams for any operating point of the system are calculated using interpolation of thermodynamic tables [25]. The system is fed with ethanol and water (1:3) both in liquid phase and ambient temperature. Inlet air was considered as an ideal gas consisting of 21% O_2 and 79% N_2. All exhaust products were also considered as ideal gases and their composition was calculated taking into account the reactions occurred in each position. The programming environment was MATLAB. Simplified models similar to the ones used in references [26–28] have been used for the turbo machines as well as for heat exchangers, since the focus was given to compare the exergetic performance of a SOFC alone or incorporated with a GT rather than to investigate part load behavior of a SOFC-GT system.

3.1. Solid Oxide Fuel Cell

Although SOFC is fed with a mixture of H_2, CO_2 and H_2O, H_2 is the only reacting component with a Lower Heating Value (LHV_{H2}) of 121,000 kJ/kg calculated from the reaction of hydrogen combustion applying thermodynamic rules [29].

The reactions taking place are:

$$\text{Anode Reaction: } 2H_2 + 2O^{2-} \rightarrow 2H_2O + 4e^- \quad (1)$$

$$\text{Cathode Reaction: } O_2 + 4e^- \rightarrow 2O^{2-} \quad (2)$$

$$\text{Overall Cell Reaction: } 2H_2 + O_2 \rightarrow 2H_2O \quad (3)$$

Defining the current density i as electron transfer rate per unit activation area of the fuel cell, V the cell voltage and A_C the activation area, the fuel cell power can be calculated through the relation:

$$\dot{W}_{FC} = iVA_C \quad (4)$$

The stoichiometric amounts of air and hydrogen mass flows in the systems examined are calculated through the following relations [30]:

$$\dot{m}_{air,stoic} = 3.57 \times 10^{-7} \frac{\dot{W}_{FC}}{V} \quad (5)$$

$$\dot{m}_{H_2,consumed} = 1.05 \times 10^{-8} \frac{\dot{W}_{FC}}{V} \quad (6)$$

Since hydrogen from the fuel and oxygen from the air are not completely consumed by the electrochemical reactions, the actual mass flows of fuel (anode inlet) and air (cathode inlet) can be determined from the fuel (U_f) and air (U_a) utilization factors expressed as below:

$$U_a = \frac{\dot{m}_{O_2,consumed}}{\dot{m}_{O_2,in}} = \frac{\dot{m}_{air,stoic}}{\dot{m}_{air}} \quad (7)$$

$$U_f = \frac{\dot{m}_{H_2,consumed}}{\dot{m}_{H_2,in}} \quad (8)$$

Utilization (U) refers to the fraction of the total fuel or oxidant introduced into a fuel cell that reacts electrochemically. The amount of hydrogen (produced in reformer device) that is electrochemically oxidized in fuel cell is related to the fuel utilization factor (U_f) and produces heat and electrical power. Through this reaction oxygen from air is consumed, water is produced and the unreacted hydrogen is directed to the burner device. Applying the first Law of Thermodynamics to the SOFC device, an energy balance relationship results, as presented in Equation (9):

$$H_3 + H_{11} + U_f \dot{m}_{H_2} LHV_{H_2} - H_4 - \dot{W}_{FC} = 0 \tag{9}$$

where:

$$H_3 = \left[\dot{m}_{O_2} h_{O_2} + \dot{m}_{N_2} h_{N_2} \right]_{T_3} \tag{10}$$

$$H_{11} = \left[(1 - U_f) \dot{m}_{H_2} \cdot h_{H_2} + \dot{m}_{CO_2} \cdot h_{CO_2} \right]_{T_{11}} \tag{11}$$

$$H_4 = \left[(1 - U_f) \dot{m}_{H_2} \cdot h_{H_2} + \dot{m}_{CO_2} \cdot h_{CO_2} + \dot{m}_{H_2O} \cdot h_{H_2O} + (1 - U_a) \cdot \dot{m}_{O_2} h_{O_2} + \dot{m}_{N_2} h_{N_2} \right]_{T_4} \tag{12}$$

3.2. Burner-Reformer

The preferred ethanol steam reforming process is represented by the following endothermic reaction with the formation of CO_2 as the desired product:

$$C_2H_5OH + 3H_2O \rightarrow 2CO_2 + 6H_2 - 173 \text{ kJ/kmol} \tag{13}$$

At the chosen temperature values (550 and 600 °C) the conversion of the above reaction reaches the thermodynamically predicted values [31]. The analysis of the ethanol reforming process, which is very complex, can be greatly simplified, from the computational point of view, assuming that the ethanol steam reforming reaction is driven to completion. It is possible to use such simplification because the hydrogen produced by the reforming reactions is consumed by the electrochemical reaction and because of the high value of its equilibrium constant in the operating conditions considered [32]. In fact many studies have shown that the ethanol steam reforming reaction is driven to completion using appropriate catalysts [33–35].

The hydrogen produced in the reformer is consumed at the fuel cell for the production of electricity. The un-reacted hydrogen (in case of $U_f < 1$) reaches the burner where it is oxidized producing thermal energy. When necessary, ethanol can also be oxidized in the burner device to satisfy the required thermal energy needs:

$$C_2H_5OH + 3O_2 \rightarrow 2CO_2 + 3H_2O + 1234,855 \text{ kJ/mol} \tag{14}$$

The produced thermal energy is calculated through Equation (15):

$$\dot{Q}_B = [\dot{m}_{H_2} (1 - U_f) LHV_{H_2} + \dot{m}_{Et,B} LHV_{Et}] \eta_B \tag{15}$$

Part of the thermal energy produced from this process is required for ethanol steam reforming and is given through the following relation:

$$\dot{Q}_R = \dot{m}_{Et,R} \Delta H_{Et,R} \tag{16}$$

The energy balance for the Burner-Reformer lumped device can be expressed as:

$$H_4^* - H_5 + \dot{Q}_B - \dot{Q}_R = 0 \tag{17}$$

where:

$$H_4^* = \left[\dot{m}_{CO_2} \cdot h_{CO_2} + \dot{m}_{H_2O} \cdot h_{H_2O} + (1 - U_a) \cdot \dot{m}_{O_2} h_{O_2} + \dot{m}_{N_2} h_{N_2} \right]_{T_4} \tag{18}$$

$$H_5 = \left[\dot{m}^*_{CO_2} \cdot h_{CO_2} + \dot{m}^*_{H_2O} \cdot h_{H_2O} + \dot{m}^*_{O_2} h_{O_2} + \dot{m}_{N_2} h_{N_2} \right]_{T_5} \tag{19}$$

and $\dot{m}^*$ refers to the resulting composition after the reactions have taken place in the burner and the mixture is in equilibrium.

3.3. Compressor

The isentropic efficiency of the compressor in the SOFC-GT system is defined as follows:

$$\eta_C = \frac{h_a(T_{2s}) - h_a(T_1)}{h_a(T_2) - h_a(T_1)} \tag{20}$$

where T_{2s} represents the ideal (isentropic) temperature corresponding to pressure P_2:

$$s_a(T_{2s}) - s_a(T_1) = 0 \tag{21}$$

and the compressor's power consumption is calculated from Equation (22):

$$\dot{W}_C = \dot{m}_a (h_a(T_2) - h_a(T_1)) \tag{22}$$

3.4. Turbine

The turbine isentropic efficiency is defined from Equation (23):

$$\eta_T = \frac{h_g(T_5) - h_g(T_6)}{h_g(T_5) - h_g(T_{6s})} \tag{23}$$

where T_{6s} is the ideal (isentropic) temperature:

$$s_g(T_{6s}) - s_g(T_5) = 0 \tag{24}$$

and the turbine generated power is calculated from Equation (25):

$$\dot{W}_T = \dot{m}_g (h_g(T_5) - h_g(T_6)) \tag{25}$$

3.5. Recuperator

The recuperator effectiveness is defined as the heat that is actually transferred to the maximum heat that could be transferred given through the simplified relation:

$$\varepsilon_{Rec} = \frac{T_3 - T_2}{T_6 - T_2} \tag{26}$$

It is assumed that heat transfer from the recuperator to environment is negligible so the energy balance is:

$$\dot{m}_a(h_a(T_3) - h_a(T_2)) = \dot{m}_g(h_g(T_6) - h_g(T_7)) \quad (27)$$

3.6. Evaporator

The evaporator is modeled through equations similar to the ones used in the recuperator device:

$$\varepsilon_{Ev} = \frac{T_{10} - T_9}{T_7 - T_9} \quad (28)$$

$$\dot{m}_g(h_g(T_7) - h_g(T_8)) = H_{10} - H_9 \quad (29)$$

$$H_9 = \dot{m}_w h_w(T_9) + \dot{m}_{Et,R} h_{Et,R}(T_9) \quad (30)$$

$$H_{10} = \dot{m}_w h_w(T_{10}) + \dot{m}_{Et,R} h_{Et,R}(T_{10}) \quad (31)$$

3.7. Simulation of the Systems

In order to simulate the operation of the SOFC-GT plant, Equations (4)–(31) are used, while for the simulation of the SOFC plant operation, the same equations are used except from Equations (20)–(25) that concern the compressor and the turbine.

From both examined systems, the overall work output that is finally utilized is given from the following equations:

$$\text{SOFC: } \dot{W}_{utilized} = \eta_{AC}\dot{W}_{FC} \quad (32)$$

$$\text{SOFC-GT: } \dot{W}_{utilized} = \eta_{AC}\dot{W}_{FC} + \eta_{AC}(\dot{W}_T - \dot{W}_C) \quad (33)$$

where η_{AC} represents the AC inverter efficiency.

3.8. Exergy Analysis of the Systems

It is well known that the exergy of a system is the maximum useful work that can be extracted from that system when it is brought reversibly to equilibrium with its environment. An exergy balance applied to a system provides information on the wasted work potential during a process as a result of irreversibilities (exergy destruction or lost work) defined also as second-law efficiency [3,36]. An exergy analysis is a powerful tool for optimizing thermodynamic systems and can be used to identify which components of the system are responsible for irreversibilities, or lost work. Exergetic analysis could lead to more realistic conclusions concerning the specification of design conditions than the conclusions resulting from conventional energy analysis [37].

Using Equations (4)–(33), the thermodynamic variables in each position for both systems are calculated. Exergy analysis of both cycles is carried out applying for each position Equations (34)–(36). The total exergy at a specific position (e.g., compressor outlet) has been estimated from Equation (34) and is the sum of the physical and chemical exergy of the components that are associated with their physical and chemical properties, respectively. An exergy balance for a control volume at steady state is formulated to calculate exergy destruction $\dot{E}_D$ using Equation (35). Exergy efficiency is referred to the exergetic potential of the primary fuel (standard exergy of ethanol) and is expressed through Equation (36):

$$e_i = e^{physical} + e^{chemical} = (h - h_o) - T_o(s - s_o) + \sum_i x_i e_i^{ch} - RT_o \sum_i x_i \ln x_i \quad (34)$$

$$\dot{E}_D = \left(\sum_i \dot{m}_i e_i\right)_{inlet} - \left(\sum_i \dot{m}_i e_i\right)_{exit} + \sum_j \left(1 - \frac{T_o}{T_j}\right)\dot{Q}_j - \dot{W} \quad (35)$$

$$\eta_{II} = \frac{\dot{W}_{utilized}}{\dot{E}_{supplied}} \quad (36)$$

In Equation (34), all quantities are on a "per kmol" basis, then are converted to "per kg" basis in order to be used in other equations.

4. Results and Discussion

The systems under investigation presented in Figure 1 are simulated at steady state performance. Reasonable operating parameters of the systems investigated have been adopted from the literature [13,17], and are presented in Table 1. Discussion on the parameters selection for systems with power rate in the range considered can be found in the above references. The variation of fuel cell voltage and power density with current density at 550 and 600 °C operating temperature of the fuel cell is shown in Figure 2. This information comes from existing experimental results reported in the literature [24]. The specific curves are used to define the reference cell voltage. The model also incorporates semiempirical correlations [38–40] to evaluate the effects of the operating pressure and fuel composition on the actual (final) voltage value. Higher current densities increase the irreversibilities in the cell and results in lower voltages. Concentration losses are the main reason for the low output voltages at high current densities. These losses are higher at 550 °C than at 600 °C. Points A, B, C and D distinguished in Figure 2 represent the operating points of an intermediate solid oxide fuel cell operating at 600 °C at 0.1, 1, 2 and 3 A/cm^2 respectively. In this work, the system's exergetic performance is examined at these points.

The exergy efficiency variation for both systems (SOFC-GT, SOFC) in relation to the current density and fuel utilization factor is illustrated in Figure 3. It can be observed for both systems that the exergy efficiency value approaches 60% when the fuel cell operates at very low current density and U_f approaching 90%. However, when higher current densities are required, the SOFC-GT exergetic efficiency prevails that of SOFC (close to 50% and 25% respectively at U_f = 0.90 and current density 3 A/cm^2). Two different regions can be distinguished in case of the SOFC-GT system: region A and region B. The region A represents the operating conditions where an additional amount of ethanol has to be consumed in the burner for the thermal needs of the system to be covered. Region B represents the operating area where there is no need for additional ethanol to be supplied to the burner. In this region the values of fuel utilization factor are low and the values of current density are high. When the value of the utilization factor is low additional thermal energy is provided to the system due to un-reacted hydrogen from the fuel cell which is eventually burnt in the burner device. When the value of current density is high, thermal energy sufficient to cover the thermal needs of the system is derived from the polarization losses.

Table 1. Main operating parameters of the SOFC-GT system [13,17].

Gas turbine cycle	
Compressor isentropic efficiency	0.81
Compressor pressure ratio	4
Turbine isentropic efficiency	0.84
AC generator efficiency	0.95
Burner-Reformer	
Ethanol Steam-to-Carbon Ratio	1.5
Burner efficiency	0.98
Pressure losses (%)	5
SOFC	
Air utilization factor (U_a)	0.25
Fuel utilization factor (U_f)	0.85
Pressure losses (%)	4
DC/AC conversion efficiency	0.95
Recuperator	
effectiveness	0.85
Pressure losses gas/air sides (%)	4
Ambient conditions	
Temperature (K)	288
Pressure (bar)	1.013

Figure 2. Experimental results of an IT-SOFC performance. Cell voltage and power density as function of current density at 600 and 550 °C [24].

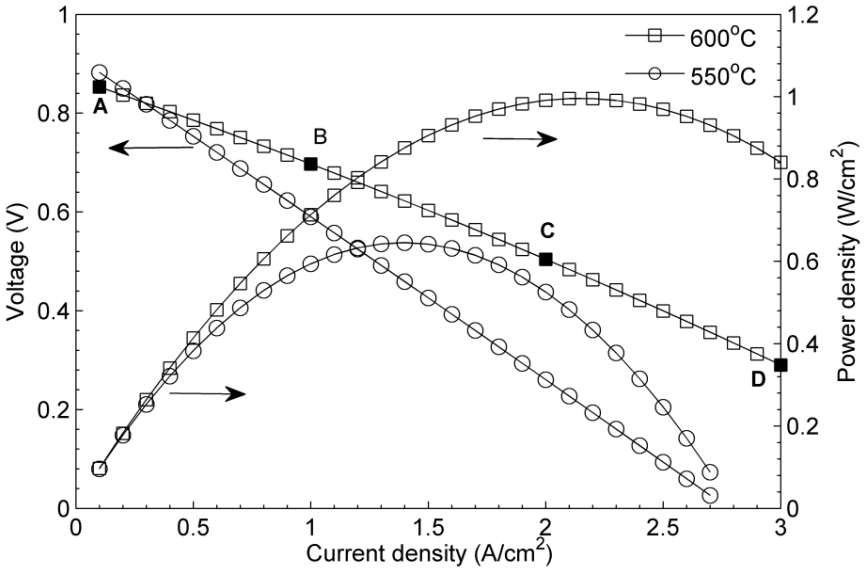

Figure 3. The effect of current density and fuel utilization factor on the efficiency of both systems; T_{FC} = 600 °C.

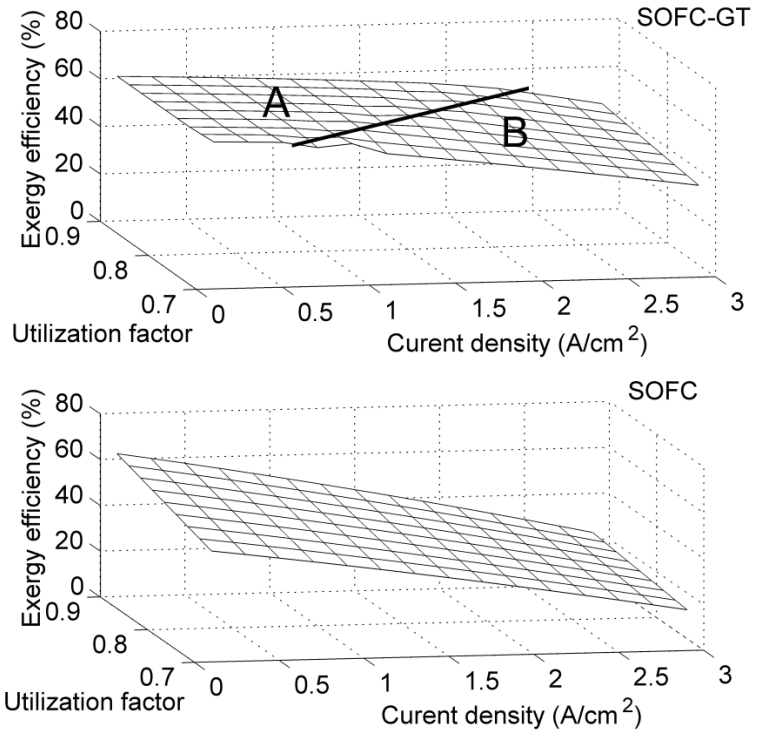

With reference to the simple SOFC system the region A decays to a single point. This means that the system operates with additional ethanol amount to the burner (region B) for all operating conditions. The exergy efficiency decreases with the increment of current density and decrement of fuel utilization factor.

The dependence of the exergy efficiency of both systems (SOFC-GT, SOFC) in relation with the current density at different values of fuel utilization factor is better illustrated in Figure 4. When the systems are operating with low fuel utilization factor, the SOFC-GT plant is more efficient than the SOFC plant. As the value of the utilization factor increases two discrete regions can be observed, limited by point I. This point depends on the fuel cell's working conditions—especially on the utilization factor—and can be defined as the equivalent point where the exergy efficiency of the SOFC-GT plant becomes equal to that of the SOFC system. In the region before point I (lower current densities) the exergy efficiency of the SOFC system is slightly higher than the efficiency of the SOFC-GT system. After this point it becomes evident that the efficiency of the SOFC-GT is higher than the efficiency of the SOFC system.

Figure 4. The effect of current density at specific values of fuel utilization factor on exergy efficiency of both systems; T_{FC} = 600 °C.

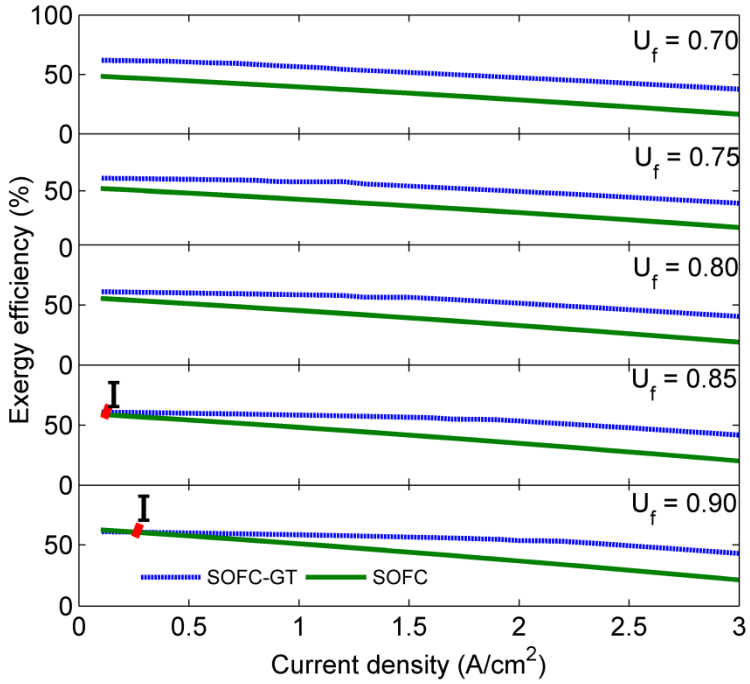

Polarization losses actually mean loss of potential useful work that is converted to heat. At the SOFC plant, polarization losses in the current density range from 0.1 to 3 A/cm^2 lead to high efficiency drop (>60%). At the SOFC-GT plant, part of the heat generated from polarization losses is further converted to useful work through the gas turbine and consequently the efficiency drop of this system is lower (<35%). It can also be observed in Figure 4 that while fuel utilization factor increases, the equivalent point described before is displaced at higher value of current density and the region where the exergy efficiency of the SOFC plant is slightly higher than the efficiency of the SOFC-GT is also extended. This is expected as the increase of the fuel utilization factor means better and more efficient fuel cell operation as un-reacted fuel decreases.

Figure 5 illustrates the effect of fuel utilization factor U_f on the exergy efficiency for both systems at specific values of current density. It is clear that the value of fuel utilization factor affects more the efficiency of the SOFC's system than the efficiency of the SOFC-GT's system, although the value of fuel utilization factor shows no impact on systems' performance when their operating points are in A region. It is also observed that the efficiency of the SOFC system is considerably lower compared to the efficiency of the SOFC-GT system at higher values of current density and the rate of efficiency reduction for the SOFC system is higher too.

Figure 5. The effect of fuel utilization factor on exergy efficiency of both systems for specific values of current density; T_{FC} = 600 °C.

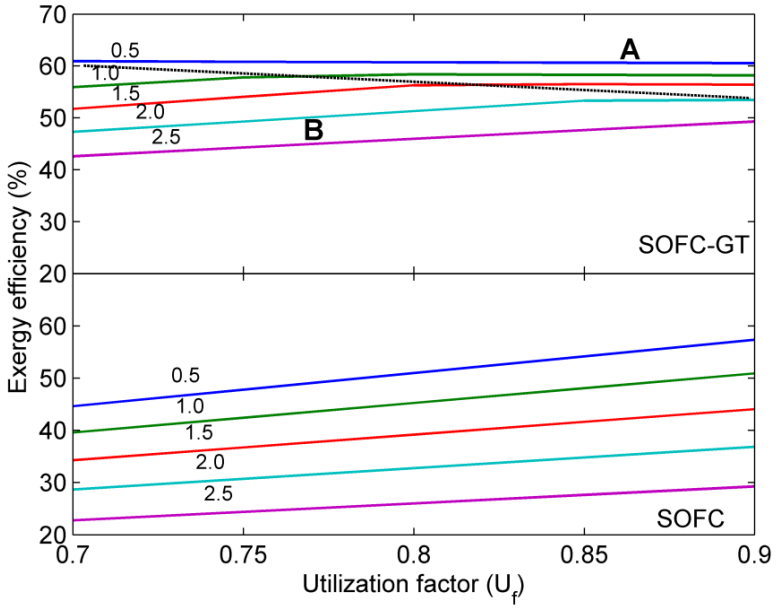

In Figure 6 the exergy efficiency of the SOFC-GT plant at 600 °C fuel cell operating temperature is compared to the one at 550 °C respectively for different values of current density and fuel utilization factor. It is observed that the system is more efficient at low values of current density and lower fuel cell operating temperature. As the value of utilization factor increases the efficiency of the plant at 550 °C is higher than the efficiency at 600 °C for a wider range of current density values. Moreover, the rate of the efficiency decrease (as the current density increases), is higher at 550 °C, as polarization losses at lower temperature occur at greater extend as illustrated in Figure 2.

Figure 6. The effect of current density, fuel utilization factor and fuel cell operating temperature on the exergy efficiency of the SOFC-GT.

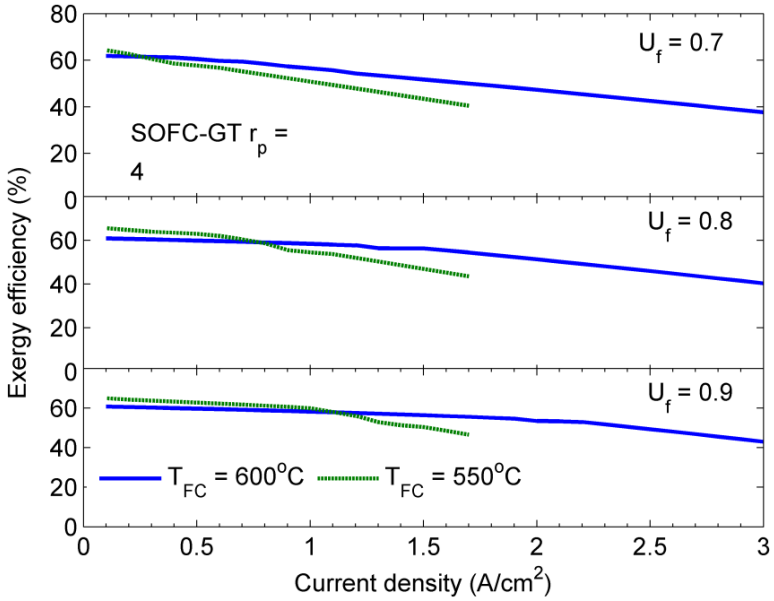

Figure 7 illustrates the turbine inlet temperature (TIT) at different values of current density and fuel utilization factor. When the SOFC-GT operates in region A (described before) TIT is almost constant at about 1200 K. In region B TIT increases with the current density and fuel utilization, reaching high values. This fact must be taken into account during system operation in order to avoid a turbine failure, especially for a turbine without blade cooling that is usually the case for small gas turbines with pressure ratio in the range considered.

Figure 7. The effect of current density and the fuel utilization factor on the gas turbine inlet temperature (TIT); T_{FC} = 600 °C and r_p = 4.

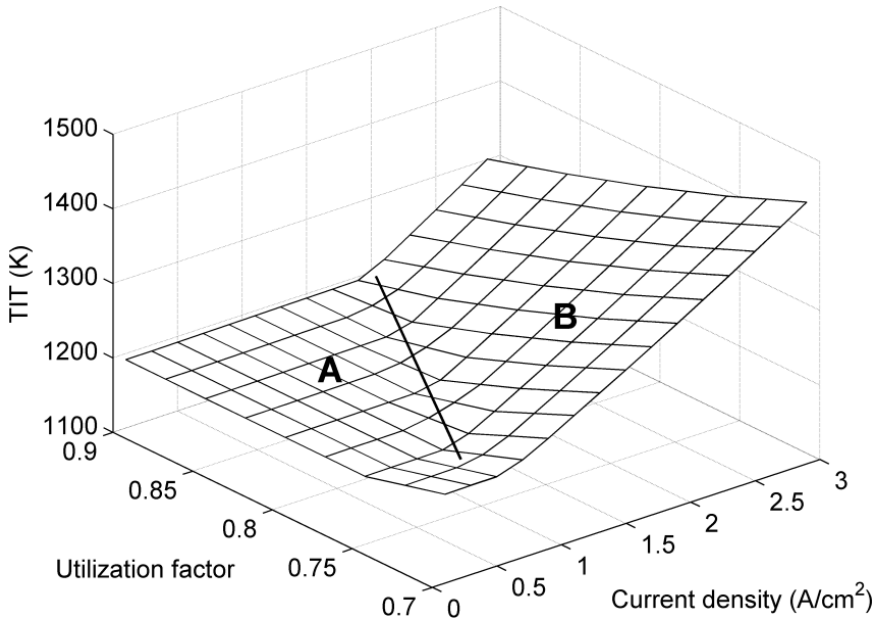

Exergy destruction rate of the systems' devices is presented in Figure 8. It is observed that for all the devices exergy destruction rate increases along with the increase of the current density. In both systems, the maximum irreversibilities occur in the fuel cell device. As it can be distinguished from Figure 8, high amounts of exergy are also destructed in the burner and the recuperator especially in the case of the SOFC system.

In Figure 9 is presented the exergy destruction rate of each device for both systems for the different fuel cell's operating points (V-I) A, B, C, D shown in Figure 2. It is obvious that the SOFC plant is more exergy destructive than the SOFC-GT plant. It is observed that as the value of current density increases the total exergy destruction rate of the SOFC plant overcomes the total exergy destruction rate of the SOFC-GT plant. When the value of current density remains low, the maximum irreversibility occurs in the burner-reformer device for the SOFC-GT system and in the fuel cell stack for the SOFC system. As the current density increases the fuel cell becomes the most exergy destructive device for both systems. At low current densities the burner–reformer device of the SOFC-GT system, where additional ethanol has to be burnt for the thermal needs of the system, is more exergy destructive than the same device at the SOFC plant. At high current densities where there is no need for additional heat, the exergy destruction rate in the burner-reformer device becomes equal for both systems. The exergy destruction rate of the compressor, the turbine and the evaporator is low

comparing to the other devices. Additionally the exergy destruction rate of the recuperator of the SOFC plant is approximately three times higher than the one of the SOFC-GT.

Figure 8. The effect of current density on exergy destruction of SOFC-GT's and SOFC's devices; T_{FC} = 600 °C and U_f = 0.85.

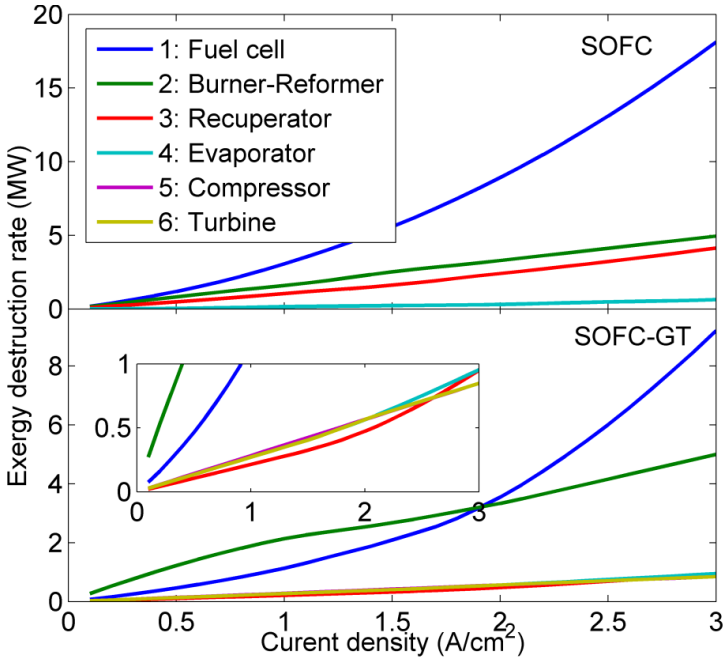

Figure 9. Exergy destruction of SOFC-GT's and SOFC's devices; T_{FC} = 600 °C and U_f = 0.85.

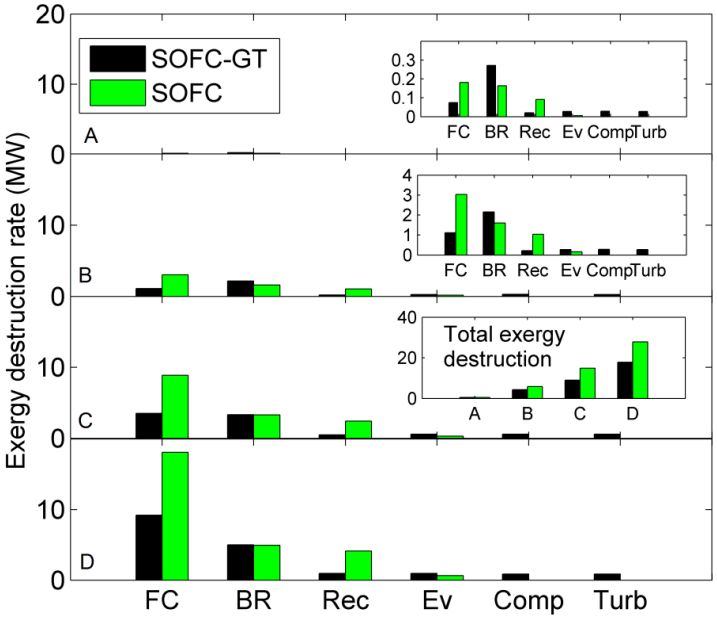

The total power produced from the SOFC-GT system is illustrated in Figure 10. At higher values of current density, power output increases with the decrease of utilization factor as gas turbine has a significant contribution to the total power output. At lower values of current density the SOFC-GT system's power output seems to be insensitive to the change of fuel utilization factor. Maximum power output occurs at higher current densities for decreasing fuel utilization factors.

Figure 10. The effect of current density and fuel utilization factor on the total power output of the SOFC-GT; T_{FC} = 600 °C and r_p = 4.

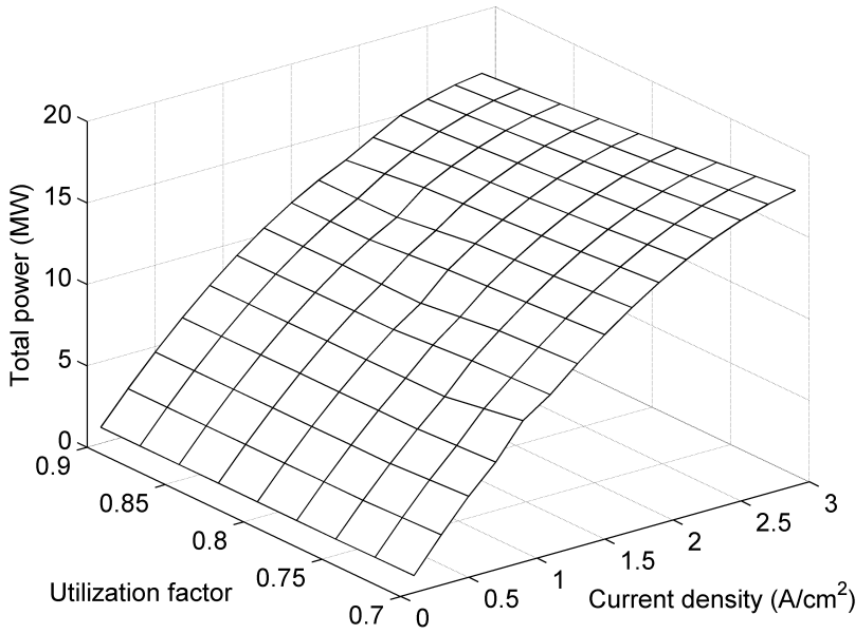

Figure 11. The effect of current density and fuel utilization factor on the power output of the SOFC device, on the total power output of the SOFC-GT, and on the fuel consumption; T_{FC} = 600 °C.

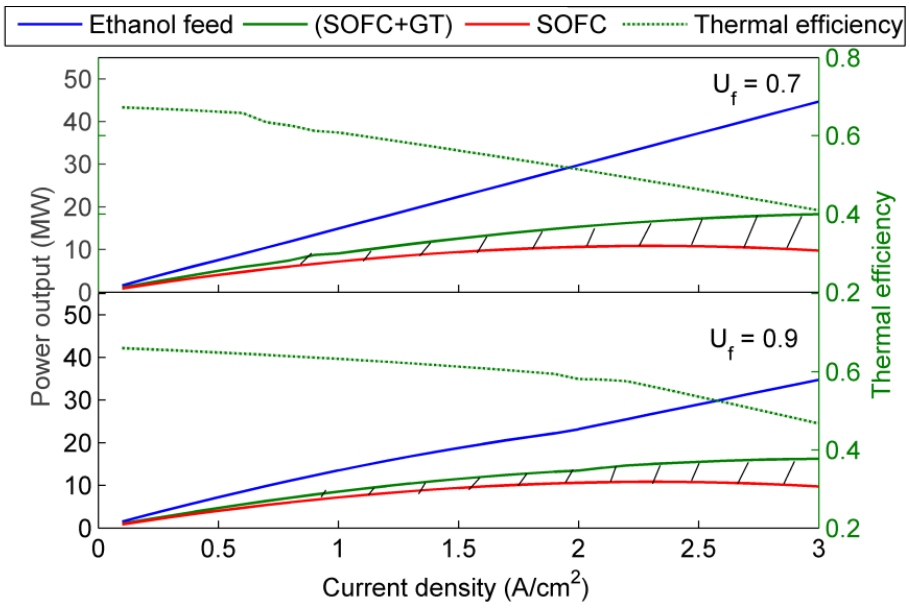

In order to be better understood the operation of the SOFC-GT system, the effect of current density on: (a) the total ethanol consumption (in terms of power), (b) the power produced from the SOFC device and (c) the total power produced (sum of the power produced from the SOFC and the Gas Turbine device) is presented in Figure 11, for utilization factors of 0.7 and 0.9, respectively. The marked region represents the power produced by the gas turbine. In other words the power contribution of the gas turbine to the total power output from the SOFC-GT system. It is clear that as

the current density increases and/or the U_f decreases, the gas turbine's power output increases, while the fuel cell's power output remains constant.

Finally, in Figure 12 the effect of current density and utilization factor on the ethanol rate consumption (in terms of kgs per second): (a) in the reformer, (b) in the burner and (c) in the SOFC-GT system (total rate) is illustrated. The ethanol is consumed in the reformer for hydrogen production and as it can be distinguished in Figure 12a, its rate increases as the current density increases. Moreover, at high current density values, as the utilization factor decreases—unreacted hydrogen increases—the ethanol consumption rate becomes higher. In Figure 12b, the rate of ethanol consumption in the burner device as a function of current density and utilization factor is depicted. It can be seen that at high current densities and low U_f, no ethanol is required for the burner. As discussed above, in this case the rate of the heat production in the fuel cell device (polarization losses) is high enough to support the whole system's energy requirements. On the other hand, when the fuel cell operates at low current densities and high utilization factor values, ethanol supply is necessary. Figure 12c simply depicts the total ethanol consumption rate (sum of ethanol consumption rate in the burner and the reformer device) as a function of current density and utilization factor.

Figure 12. The effect of current density and fuel utilization factor on the ethanol consumption rate in: (**a**) the reformer, (**b**) the burner, (**c**) the whole SOFC-GT system; T_{FC} =600 °C and r_p = 4.

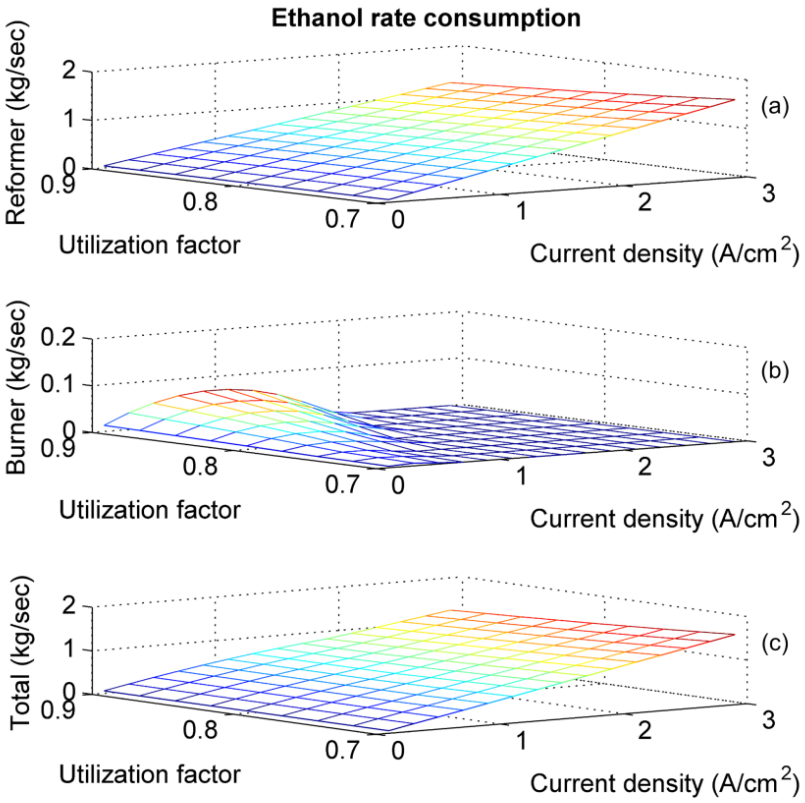

5. Conclusions

In this work two Solid Oxide Fuel Cell based systems (SOFC-GT and SOFC) are exergetically analyzed and compared. It was found that for both cases the exergy efficiency value approaches 60% when the fuel cell operates at very low current density values and high utilization factor. However, when higher current densities are required, the SOFC-GT exergetic efficiency prevails that of the SOFC. Moreover, when the systems are operating with low fuel utilization factor, SOFC-GT plant is more efficient than the SOFC plant. As the utilization factor increases there is a region in which the later becomes more efficient than the former. This region increases as the U_f increases. Additionally, it is also concluded that only at low values of current density lower operating fuel cell temperature leads to higher efficiency for both plants.

Acknowledgments

Finally, for the financial support, P. Tsiakaras is grateful to the Greek Ministry of Development-GSRT "SYNERGASIA" Program (09SYN-32-615: ECHOCO2) and F. Tzorbatzoglou is grateful to the Research Funding Program: Heracleitus II of the Operational Programme "Educational and Lifelong Learning" which is co-funded by the European Union (European Social Fund) and National Resources.

References

1. Dunn, S. Hydrogen futures: Toward a sustainable energy system. *Int. J. Hydrog. Energy* **2002**, *27*, 235–264.
2. Cherry, R.S. A hydrogen utopia? *Int. J. Hydrog. Energy* **2004**, *29*, 125–129.
3. Silveira, J.L.; Braga, L.B.; de Souza, A.C.C.; Antunes, J.S.; Zanzi, R. The benefits of ethanol use for hydrogen production in urban transportation. *Renew. Sust. Energ. Rev.* **2009**, *13*, 2525–2534.
4. Douvartzides, S.; Coutelieris, F.; Tsiakaras, P. Exergy analysis of a solid oxide fuel cell power plant fed by either ethanol or methane. *J. Power Sources* **2004**, *131*, 224–230.
5. Recknagle, K.P.; Williford, R.E.; Chick, L.A.; Rector, D.R.; Khaleel, M.A. Three-dimensional thermo-fluid electrochemical modeling of planar SOFC stacks. *J. Power Sources* **2003**, *113*, 109–114.
6. Padullés, J.; Ault, G.W.; McDonald, J.R. An integrated SOFC plant dynamic model for power systems simulation. *J. Power Sources* **2000**, *86*, 495–500.
7. Campanari, S.; Iora, P. Definition and sensitivity analysis of a finite volume SOFC model for a tubular cell geometry. *J. Power Sources* **2004**, *132*, 113–126.
8. Chan, S.H.; Ho, H.K.; Tian, Y. Multi-level modeling of SOFC–gas turbine hybrid system. *Int. J. Hydrog. Energy* **2003**, *28*, 889–900.
9. Kandepu, R.; Imsland, L.; Foss, B.A.; Stiller, C.; Thorud, B.; Bolland, O. Modeling and control of a SOFC-GT-based autonomous power system. *Energy* **2007**, *32*, 406–417.
10. Song, T.W.; Sohn, J.L.; Kim, T.S.; Ro, S.T. Performance characteristics of a MW-class SOFC/GT hybrid system based on a commercially available gas turbine. *J. Power Sources* **2006**, *158*, 361–367.

11. Yi, Y.; Rao, A.D.; Brouwer, J.; Samuelsen, G.S. Analysis and optimization of a solid oxide fuel cell and intercooled gas turbine (SOFC–ICGT) hybrid cycle. *J. Power Sources* **2004**, *132*, 77–85.
12. Calise, F.; Palombo, A.; Vanoli, L. Design and partial load exergy analysis of hybrid SOFC–GT power plant. *J. Power Sources* **2006**, *158*, 225–244.
13. Haseli, Y.; Dincer, I.; Naterer, G.F. Thermodynamic analysis of a combined gas turbine power system with a solid oxide fuel cell through exergy. *Thermochim. Acta* **2008**, *480*, 1–9.
14. Vinni, C.; Stamatis, A.; Tsiakaras, P. An Exergetic Analysis of an Ethanol Fed SOFC-GT Hybrid System. In *Proceedings of the 3rd European Fuel Cell Technology & Applications Conference—Piero Lunghi Conference (EFC)*, 15–18 December, Rome, Italy, 2009.
15. Massardo, A.F.; Lubelli, F. Internal reforming solid oxide fuel cell-gas turbine combined cycles (IRSOFC-GT): Part A—Cell model and cycle thermodynamic analysis. *J. Eng. Gas. Turb. Power* **2000**, *122*, 27–35.
16. Srisiriwat, A. High Temperature Solid Oxide Fuel Cell Integrated with Autothermal Reformer. In *Proceedings of the IEEE 2nd International Power and Energy Conference (PECon)*, Johor Bahru, Malaysia, 1–3 December 2008.
17. Cocco, D.; Tola, V. Use of alternative hydrogen energy carriers in SOFC–MGT hybrid power plants. *Energy Convers. Manag.* **2009**, *50*, 1040–1048.
18. Douvartzides, S.L.; Coutelieris, F.A.; Tsiakaras, P.E. On the systematic optimization of ethanol fed SOFC-based electricity generating systems in terms of energy and exergy. *J. Power Sources* **2003**, *114*, 203–212.
19. Assabumrungrat, S.; Pavarajarn, V.; Charojrochkul, S.; Laosiripojana, N. Thermodynamic analysis for a solid oxide fuel cell with direct internal reforming fueled by ethanol. *Chem. Eng. Sci.* **2004**, *59*, 6015–6020.
20. Jamsak, W.; Assabumrungrat, S.; Douglas, P.L.; Laosiripojana, N.; Suwanwarangkul, R.; Charojrochkul, S.; Croiset, E. Performance of ethanol-fuelled solid oxide fuel cells: Proton and oxygen ion conductors. *Chem. Eng. J.* **2007**, *133*, 187–194.
21. Casas, Y.; Arteaga, L.E.; Morales, M.; Rosa, E.; Peralta, L.M.; Dewulf, J. Energy and exergy analysis of an ethanol fueled solid oxide fuel cell power plant. *Chem. Eng. J.* **2010**, *162*, 1057–1066.
22. Zhe, Y.; Qizhao, L.; Zhu, B. Thermodynamic analysis of ITSOFC co-generation system fueled by ethanol. *Int. J. Energy Res.* **2011**, *35*, 1025–1031.
23. Pikalova, E.Y.; Maragou, V.I.; Demina, A.N.; Demin, A.K.; Tsiakaras, P.E. The effect of co-dopantaddition on the properties of $Ln_{0.2}Ce_{0.8}O_{2-\delta}$ (Ln = Gd, Sm, La) solid-state electrolyte. *J. Power Sources* **2008**, *181*, 199–206.
24. Shao, Z.; Haile, S.M. A high-performance cathode for the next generation of solid-oxide fuel cells. *Nature* **2004**, *431*, 170–173.
25. Cengel, Y.A.; Boles, A.M. *Thermodynamics: An Engineering Approach*, 5th ed.; McGraw-Hill: New York, NY, USA, 2006.
26. Akkaya, A.V.; Sahin, B.; Huseyin Erdem, H. Exergetic performance coefficient analysis of a simple fuel cell system. *Int. J. Hydrog. Energy* **2007**, *32*, 4600–4609.
27. Haseli, Y.; Dincer, I.; Naterer, G.F. Thermodynamic modeling of a gas turbine cycle combined with a solid oxide fuel cell. *Int. J. Hydrog. Energy* **2008**, *33*, 5811–5822.

28. Park, S.K.; Oh, K.S.; Kim, T.S. Analysis of the design of a pressurized SOFC hybrid system using a fixed gas turbine design. *J. Power Sources* **2007**, *170*, 130–139.
29. Smith, J.M.; van Ness, H.C.; Abbot, M.M. *Introduction to Chemical Engineering Thermodynamics*, 6th ed.; McGraw-Hill: New York, NY, USA, 2001.
30. Larminie, J.; Dicks, A. *Fuel Cells Systems Explained*, 2nd ed.; John Wiley and Sons Ltd.: Sussex, UK, 2003.
31. Zhang, B.; Cai, W.; Li, Y.; Xu, Y.; Shen, W. Hydrogen production by steam reforming of ethanol over an Ir/CeO_2 catalyst: Reaction mechanism and stability of the catalyst. *Int. J. Hydrog. Energy* **2008**, *33*, 4377–4386.
32. Contreras, J.L.; Salmones, J.; García, L.A.; Ponce, A. ; Zeifert, B.; Fuentes, G.A. Hydrogen production by ethanol steam reforming over co-hydrotalcites having basic sites. *J. New Mater. Electrochem. Syst.* **2008**, *11*, 109–117.
33. Li, M.; Wang, X.; Li, S.; Wang, S.; Ma, X. Hydrogen production from ethanol steam reforming over nickel based catalyst derived from Ni/Mg/Al hydrotalcite-like compounds. *Int. J. Hydrogen Energy* **2010**, *35*, 6699–6708.
34. Ma, H.; Zhang, R.; Huang, S.; Chen, W.; Shi, Q. Ni/Y_2O_3-Al_2O_3 catalysts for hydrogen production from steam reforming of ethanol at low temperature. *J. Rare Earth.* **2012**, *30*, 683–690.
35. Wu, Y.J.; Díaz Alvarado, F.; Santos, J.C.; Gracia, F.; Cunha, A.F.; Rodrigues, A.E. Sorption-enhanced steam reforming of ethanol: Thermodynamic comparison of CO_2 sorbents. *Chem. Eng. Technol.* **2012**, *35*, 847–858.
36. Kotas, T.J. *The Exergy Method of Thermal Plant Analysis*; ButterWorth-Heinemann Ltd.: London, UK, 1985.
37. Hotz, N.; Senn, S.M.; Poulikakos, D. Exergy analysis of a solid oxide fuel cell micropowerplant. *J. Power Sources* **2006**, *158*, 333–347.
38. *Fuel Cell Handbook*, 5th ed.; EG&G Services Parsons, Inc., Science Applications International Corporation: Morgantown, WV, USA, 2000.
39. Campanari, S. Thermodynamic model and parametric analysis of a tubular SOFC module. *J. Power Sources* **2001**, *92*, 26–34.
40. Zhang, W.; Croiset, E.; Douglas, P.L.; Fowler, M.W.; Entchev, E. Simulation of a tubular solid oxide fuel cell stack using AspenPlusTM unit operation models. *Energy Convers. Manag.* **2005**, *46*, 181–196.